

UWL REPOSITORY

repository.uwl.ac.uk

Imaging microstructure of the barley rhizosphere: particle packing and root hair influences

Koebernick, Nicolai, Daly, Keith R., Keyes, Samuel D., Bengough, Anthony G., Brown, Lawrie K., Cooper, Laura J., George, Timothy S., Hallett, Paul D., Naveed, Muhammad ORCID: https://orcid.org/0000-0002-0923-4976, Raffan, Annette and Roose, Tiina (2018) Imaging microstructure of the barley rhizosphere: particle packing and root hair influences. New Phytologist, 221 (4). pp. 1878-1889. ISSN 0028-646X

http://dx.doi.org/10.1111/nph.15516

This is the Accepted Version of the final output.

UWL repository link: https://repository.uwl.ac.uk/id/eprint/5489/

Alternative formats: If you require this document in an alternative format, please contact: <u>open.research@uwl.ac.uk</u>

Copyright:

Copyright and moral rights for the publications made accessible in the public portal are retained by the authors and/or other copyright owners and it is a condition of accessing publications that users recognise and abide by the legal requirements associated with these rights.

Take down policy: If you believe that this document breaches copyright, please contact us at <u>open.research@uwl.ac.uk</u> providing details, and we will remove access to the work immediately and investigate your claim.



DR TIINA ROOSE (Orcid ID : 0000-0001-8744-2060)

Article type : Regular Manuscript

Imaging microstructure of the barley rhizosphere: particle packing and root hair influences

Nicolai Koebernick¹, Keith R. Daly¹, Samuel D. Keyes¹, Anthony G. Bengough^{2,3}, Lawrie K. Brown², Laura J. Cooper^{1,4}, Timothy S. George², Paul D. Hallett⁵, Muhammad Naveed^{5,6}, Annette Raffan⁵, and Tiina Roose^{1\$}

 ¹Bioengineering Sciences Research Group, Engineering Sciences Academic Unit, Faculty of Engineering and the Environment, University of Southampton, Southampton SO17 1BJ, UK
 ²Ecological Sciences Group, The James Hutton Institute, Dundee DD2 5DA, UK
 ³School of Science and Engineering, University of Dundee, Dundee DD1 4HN, UK
 ⁴Mathematics Institute, University of Warwick, Warwick CV4 7AL, UK
 ⁵Institute of Biological and Environmental Science, University of Aberdeen, Aberdeen AB24 3FX, UK
 ⁶School of Computing and Engineering, University of West London, London W5 5RF, UK

^{\$} Corresponding author: T.Roose@soton.ac.uk, Faculty of Engineering and Environment, University of Southampton, University Road, SO17 1BJ Southampton, United Kingdom. Phone: +44 (0)23 8059 5000. ORCID: 0000-0001-8710-1063

Received: 12 June 2018 Accepted: 23 September 2018

Summary

- Soil adjacent to roots has distinct structural and physical properties from bulk soil, affecting
 water and solute acquisition by plants. Detailed knowledge on how root activity and traits
 such as root hairs affect the 3D pore structure at a fine scale is scarce and often
 contradictory.
- Roots of hairless barley (*Hordeum vulgare* L. cv 'Optic') mutant (NRH) and its wildtype (WT) parent were grown in tubes of sieved (<250 μm) sandy loam soil under two different water regimes. The tubes were scanned with synchrotron based X-ray CT to visualise pore

This article has been accepted for publication and undergone full peer review but has not been through the copyediting, typesetting, pagination and proofreading process, which may lead to differences between this version and the Version of Record. Please cite this article as doi: 10.1111/nph.15516

structure at the soil-root interface. Pore volume fraction and pore size distribution were analysed versus distance within 1 mm of the root surface.

- Less dense packing packing of particles at the root-surface was hypothesised to cause the
 observed increased pore volume fraction immediately next to the epidermis. The pore size
 distribution was narrower due to a decreased fraction of larger pores. There were no
 statistically significant differences in pore structure between genotypes or moisture
 conditions.
- A model is proposed that describes the variation in porosity near roots taking into account soil compaction and the surface effect at the root surface.

Keywords: Root hairs, rhizosphere, *Hordeum vulgare*, noninvasive imaging, synchrotron, soil structure, particle packing

Introduction

The geometry of the available pore space in soil is directly related to water flow and solute transport. It is well known that plant roots alter the pore geometry of the soil adjacent to roots by the combined action of mechanical and hydraulic stresses and biochemical activity (i.e. the release of exudates and the associated enhancement of microbial activity). The pore structure in the immediate vicinity of roots is of primary importance for root water and solute uptake because all resources entering or leaving the root have to cross this layer which has distinct physical and structural properties. The importance of measuring small-scale hydraulic gradients at the soil-root interface for instance, was recognized in the 1950s by Richards and Wadleigh (1952). More recent work combining imaging and modelling has shown that enhanced inter-aggregate contact caused by root expansion increased the simulated rate of root water uptake significantly (Aravena et al. 2011; Aravena et al. 2014). Despite the potential importance of the rhizosphere pore structure for resource acquisition there is still a substantive lack of understanding of the structural properties of rhizosphere soil, which mechanisms and root traits contribute to structural changes, and how the altered pore geometry affects resource capture by roots.

In order to penetrate soil, roots must exert a growth pressure that overcomes the impedance opposing root elongation (Jin et al. 2013) and radial growth. Root penetration therefore depends on soil mechanical properties such as pore structure, soil strength, and soil matric potential (Bengough et al. 2011; Valentine et al. 2012), as well as morphological properties of the roots. Thicker roots are

generally better at penetrating strong soils (Chimungu et al. 2015), indeed thickening of roots in strong soils has been interpreted as a mechanism of overcoming limiting axial stress by loosening the soil at the root tip (Hettiaratchi 1990). Furthermore, the shape of the root tip (Colombi et al. 2017b) and the release of mucilage at the root cap have been shown to influence root penetration (lijima et al. 2003; Keyes et al. 2017; Vollsnes et al. 2010). In naturally structured soils, roots can overcome high localised mechanical impedance by compensatory extension into loose soil compartments or macropores (Bingham and Bengough 2003; Colombi et al. 2017). The ability to penetrate loose soil and biopores may be enhanced by the presence of root hairs (Bengough et al. 2016). These factors are related to the deformation pattern of soil at the soil-root interface caused by root penetration into soil. The majority of previous experimental studies and physical models predict a zone of soil densification around the roots as they ingress into soil (Aravena et al. 2011; Aravena et al. 2014; Bruand et al. 1996; Hettiaratchi 1990; Vollsnes et al. 2010; Young 1998). Dexter (1987) proposed a simple model that predicted an exponential decrease of soil density with distance from the root surface. Similar patterns have been observed experimentally using time-lapse imaging techniques (Keyes et al. 2017; Vollsnes et al. 2010). However, Keyes et al. (2017) showed that vertical displacement was much stronger than lateral displacement and that particles tended to be dragged along in the direction of root growth. Recent observations by Helliwell et al. (2017), using time-lapse CT imaging, have shown that densification of rhizosphere soil may not be the general trend. They showed that soil porosity decreased with distance from the root surface of tomato. The greatest porosity gradient was observed in the youngest roots and it decreased with root maturation. Similar observations were made in an experiment comparing the rhizosphere soil structure of a root hair deficient barley mutant with its wildtype parent (Koebernick et al. 2017). While the hairless mutant exhibited decreased air-filled porosity at the soil-root interface, wildtype roots showed a significantly greater air-filled porosity at the immediate root surface. It was concluded that root hairs might play a crucial role in the regulation of pore structure in the rhizosphere, although the mechanism remained unclear. Increased porosities in the rhizosphere have been evidenced in earlier work (Feeney et al. 2006; Hallett et al. 2009) and it could be shown that roots had a much stronger impact on soil porosity than root associated fungi. Whalley et al. (2005) found no differences in porosity, but greater pore sizes in aggregates from the rhizosphere compared to those from the bulk soil. It is worth mentioning that root-soil contact can be significantly decreased when roots grow into soil with many macropores (Colombi et al. 2017; Kooistra et al. 1992; Schmidt et al. 2012) or shrink when they experience low water potentials (Carminati et al. 2013), which would result in a greater porosity close to roots.

Another mechanism that may impact porosity close to roots is mechanical fracturing of the soil by root growth or plant water uptake. Radial expansion of the root may loosen the soil ahead of the growing tip (Hettiaratchi 1990) and root growth may lead to elastic fracturing of the soil instead of plastic deformation, especially under very dry conditions (Ruiz et al. 2015). Water uptake by roots is recognised as a major driver of crack formation through shrinkage of clay particles (Yoshida and Hallett 2008). Wetting and drying cycles in the rhizosphere are also an important driver of aggregation and rhizosheath formation (Albalasmeh and Ghezzehei 2014; Watt et al. 1994), additionally requiring binding agents which are exuded by plant roots and microbes (Czarnes et al. 2000; Hallett et al. 2009; Vidal et al. 2018). These root exudates may differ significantly in their chemical composition and physical properties depending on the species and among genotypes of the same species (Mwafulirwa et al. 2016; Naveed et al. 2017a; Naveed et al. 2017b). For instance, Naveed et al. (2017a) showed that exudates from barley roots weakened soil as opposed to exudates from maize, which stabilised soil. Root exudates are an important carbon source for soil microbiota, including fungi and bacteria, which play an important role in the formation of microaggregates in the rhizosphere (Vidal et al. 2018). Microbial decomposition of root exudates may also reverse the weakening / stabilising effect of exudates (Naveed et al. 2017a).

An important aspect determining the porosity close to a root surface that has not yet received much attention is the packing of soil particles and agglomerates arranged about the root surface. Fig. 1 illustrates the concept of the surface/wall effect (Suzuki et al. 2008) where particles pack more tightly together than against larger surfaces. Immediately at the root-soil interface, this could produce particle or aggregate scale increases in porosity, which would subsequently influence local soil physical behaviour. Due to such a surface effect, radial void distribution about a root surface would be expected to take the shape of an oscillatory wave with amplitude and frequency depending on the relative diameters of the root and the soil particles. Such a phenomenon has been extensively analysed both experimentally and mathematically in packed beds of spheres in cylindrical containers such as chemical reactors (Mueller 2010; Suzuki et al. 2008), but has to our knowledge not been considered in determining porosity near biological interfaces such as plant roots.

Here, we present an imaging study with roots of contrasting barley (*Hordeum vulgare* L. cv. Optic) genotypes, a hairless mutant (NRH) and its wildtype parent (WT) grown in soil microcosms to visualise the impact of root activity on soil pore structure at the soil-root interface. Two contrasting moisture treatments were compared to assess the impact of soil suction on rhizosphere structure formation. Digital image analysis was applied to extract soil structural parameters with distance

from the roots. We propose a novel simplified model of porosity distribution in the rhizosphere, which takes into account soil compression by root extension and the particle packing geometry of spherical soil particles about the root surface. Our findings have implications on the dynamics of water and solute flow across the rhizosphere, which may affect plant productivity.

Materials and Methods

Sample preparation

The soil was a sandy loam textured Dystric Cambisol collected at South Bullionfield at the James Hutton Institute, Dundee, UK. The soil was air dried and sieved to <250 µm. We selected a finer particle size range than our earlier work (Koebernick et al. 2017) to explore the capacity of roots to aggregate soil, rather than deform and restructure an aggregate bed, and to achieve consistent packing in the root microcosms. To ensure even watering with a controlled water potential, 25 cm long strings of carbon fibre wick ($\phi = 1$ mm) were tied to a knot on one end and passed through a 1 mL syringe barrel (ϕ = 4.2mm) such that they did not slip through the syringe nozzle. A 1mm layer of fine sand was poured into the syringe barrel via a funnel. Next, the soil was packed into the syringe barrel by passing it through the funnel until the syringe barrel was completely filled with soil. The soil was consolidated by gently tapping the syringe barrel three times with a spatula. The freed up space was refilled with soil and gently tapped again. This procedure resulted in a homogeneous packing at a dry bulk density of 1.31 ± 0.03 Mg m⁻³. This soil typically has a bulk density of 1.2 Mg m⁻³ in the field immediately after tillage, but this includes macropores that do not exist in our study due to the particle size range studied and intentional removal of larger aggregated structures. Individual syringe barrels were clustered in groups of seven and connected to a 3D printed seedling assembly as described in Koebernick et al. (2017).

The seed compartment of the seedling assembly was filled with fine sand and watered to a gravimetric water content of 0.2 g g⁻¹. A total of 30 assemblies were prepared and placed into two sample holder racks. Watering of the syringe barrels was provided by hanging the wicks into open water reservoirs at a distance of 20 cm resulting in a head of -2 kPa at the bottom of the syringes. Two contrasting moisture treatments were used, i) a constant treatment ("wet"), where reservoirs were kept continuously under the sample holder rack, and ii) a cycle of wetting and drying ("wet-dry"), generated by removing the reservoir every second day and then replacing after 24 hours. One of three plant treatments was randomly assigned to each assembly: i) a root hair bearing wild-type (WT) of barley (*Hordeum vulgare* L. cv. Optic), ii) a hairless mutant (NRH), and iii) unplanted controls.

Seeds were obtained from the barley mutant population at The James Hutton Institute (Caldwell et al. 2004) described previously by (Brown et al. 2012). The resulting experimental design was a 2 × 3 factorial design with 2 levels for moisture treatment (wet, wet-dry), 3 levels for plant treatment (WT, NRH, control) and 5 replicates per condition. One pre-germinated seed was placed in each seed compartment of the planted conditions. Seed compartments were sealed with cling film until emergence of the seedlings. After removal of the cling film, another 2 ml of water per day were pipetted into each seed compartment. Plants were grown for 12 d in a climate chamber (Conviron Ltd., Winnipeg, Canada) operating with a photoperiod of 14 h, temperature of 23°/18° C during day and night, respectively, relative humidity of 75%, and at 500 μ mol m⁻² s⁻¹ photosynthetic photon flux density during the day.

Synchrotron based X-ray CT scanning

Synchrotron based X-ray CT scanning (SRCT) was performed at the I13 beamline at Diamond Light Source, Oxfordshire, UK. Plants were carried live to the beamline and individual syringe barrels were excised from the growth assembly and sealed with parafilm. Syringe barrels were scanned at two different heights (3.5 mm apart) near the upper end of the syringe barrel to maximise the chance of finding roots. Scans were conducted using 'pink light' at energies of ca. 15-20 keV. A total of 1601 projections through 180° were recorded with an exposure time of 0.15 s leading to a total duration of ~4 min per scan. X-rays were scintillated using a 500 μ m cadmium tungstate (CdWO₄) scintillator. The scintillated light was magnified using a microscope system (4× optical magnification) and recorded with a PCO edge 5.5 CMOS detector. Resulting pixel size was 1.6 μ m with a field of view (FOV) of 4 × 3.5 mm. Reconstruction of 3D images was carried out with a filtered back-projection algorithm and converted to stacks of 2160 slices, each comprising 2560 × 2560 pixels with 32-bit dynamic range. After scanning, syringes were snap frozen and stored at -80° C for water content measurements. Water content was measured by weighing the soil in each syringe before and after oven drying at 80° C for 48 h. Shoot length and fresh weight was recorded on excised shoots. Root hair morphology was measured on washed out roots of three selected samples using a light microscope. Roots were washed out from the syringe barrels and sonicated for 5 mins to remove adhered soil particles. Roots were placed on microscope slides and imaged with a light microscope at 4 × magnification.

Image analysis

All image processing and analysis steps were performed in ImageJ (Schindelin et al. 2012) and Matlab 2016a (The MathWorks Inc., Cambridge, UK). In the reconstructed CT volumes, a systematic drop off of grey values at the edge of the syringe barrels (Fig. 1) could be observed. Additionally, in many of the syringes, roots grew close to the syringe walls. These samples were excluded from further analysis by selecting only those images, where roots were growing within a cylinder of 3.8 mm from the centre of the syringe. This region was defined by calculating a projection along the zaxis of the CT images (see supporting information, Fig. S2), and measuring the average grey value with distance from the centre. Due to the fine textured nature of the soil used in this study, it was impossible to segment the root hairs as was done in previous studies (Keyes et al. 2013; Koebernick et al. 2017).

For one treatment combination (*WT wet-dry*) only 4 replicates fulfilled the filtering criteria, for all others there were at least 5 replicates. For treatment combinations where more than 5 replicates fulfilled the requirements, 5 were chosen randomly using a random number generator. Image contrast was enhanced using histogram equalization. Images were downscaled in the x,- y-, and z-directions, respectively, by a factor of 2 to reduce computational costs. This resulted in a FOV of 1280×1280×1079 voxels at isotropic voxel size of 3.2 μ m. Downscaling effectively applied a mean filter with a σ =1 voxel radius. Soil was segmented into pore and solid phases using Otsu's method (Otsu 1979). The threshold was determined on a reference volume generated from 20 random slices from each of the 29 replicate scans. The identical threshold was applied to all images for segmentation of pores. A 3D median filter (σ =2 voxels) was applied on the resulting binary images (Fig. 3c). For the quantification of pore size distribution, the "local thickness" tool in ImageJ was applied on the binary images (Fig. 3d, Fig.5).

For the segmentation of roots, the images were further downscaled by a factor of 2. A 3D median filter (σ =2 voxels) was applied and a global threshold was computed using Otsu's method. Subsequently, an open-close operation was performed using an octagonal structuring element with a radius of σ =4 voxels. The particle analyser in ImageJ was used to remove any particles with a volume of less than 50000 voxels. The resulting image was then upscaled by a factor of 2 (Fig. 3b). A 3D Euclidean distance transform was applied to the segmented root image to determine the distance of any soil voxel to the root surface. Pore volume fraction and pore size distribution changes with distance from the root were recorded within non-overlapping annuli of 32-µm thickness (i.e. 10 voxels) about the root. To minimise any edge effects imposed by the syringe walls,

only the quadrant furthest from the wall was analysed. Pore volume fraction was recorded as the volume of detected pores divided by the volume of the analysed region.

Three light microscope images of selected WT samples were analysed for root hair morphology. Root hair density was estimated by counting root hairs along a 1 mm root segment in three micrographs. Root hair length was measured with the segmented line tool for n=18 selected root hairs in ImageJ.

Analysis of porosity variation about the root

The variation of pore volume fraction about the root surface was analysed using a new modified model that accounts for the variation of void distribution caused by the surface/wall effect at the root surface. It is assumed that the variation in porosity at the root surface is related to the packing geometry of particles against a surface. For simplicity, the model soil used to illustrate this point is composed of large, mono-sized spherical rigid particles of radius r_p and a sub resolution mixed phase with porosity ϕ_m . In soils a wider range of soil particle sizes and shapes may diminish the impact of the surface/wall effect, but it is expected to have a major influence right at the root-soil interface.

It is assumed that the soil particles form a hexagonal sphere packing, illustrated in 2D in Figure 1. When observing the porosity ϕ at a distance $r - r_0$ from the root (green line in Figure 1) it can be seen that ϕ oscillates due to the varying volume fraction taken up by the large soil particles, red dashed line in Figure 1. This oscillatory behaviour will occur everywhere except immediately adjacent to the root, where the surface/wall effect of the root surface forces an incomplete sphere packing. At this point porosity increases due to the absence of soil particles in the region occupied by the root. Calculating the porosity as a function of distance from the root can be achieved by considering the region of space occupied by the large spherical soil particles as a function of distance from the root. In order to simplify the approximation only the increase in porosity immediately adjacent to the root is considered and the oscillations in porosity further from the root are neglected. The result is a modified expression for the porosity

$$\phi = \left[\phi_b - \phi_m \left(1 - \frac{\pi}{2\sqrt{3}}\right)\right] \left(1 - e^{-k\frac{(r-r_0)}{r_0}}\right) + \phi_{AD},\tag{1}$$

where

$$\phi_{AD} = \begin{cases} \phi_m \left(1 - \frac{\pi}{2\sqrt{3}} \frac{r_p^2 - (r_p + r_0 - r)^2}{r_p^2} \right) & r_0 \le r \le (r_0 + r_p) \\ \phi_m \left(1 - \frac{\pi}{2\sqrt{3}} \right) & r > (r_0 + r_p) \end{cases}$$
(2)

where ϕ_b is the bulk porosity, k is the Dexter decay constant and r_0 is the root radius. The equation is constrained such that the gradient at $r = r_0$ is negative, which amounts to the condition

$$\phi_m = \frac{2\phi_b k r_p}{r_0 \pi} + \delta, \tag{3}$$

where $\delta > 0$ is a fitting parameter. The result is a set of 5 fitting parameters r_0 , r_p , ϕ_b , k, and δ . Experimental data were fitted using Dexter's (1987) model and the new, modified approach using a nonlinear solver in Matlab.

Analysis of pore size distribution

Pore size distribution was derived from the histogram of the 'local thickness' map within the analysed region. To analyse any changes in pore size distribution between treatments and with distance from the root the van Genuchten model was used, i.e., the water release curve is given by

$$S_e = \frac{(\theta - \theta_r)}{(\theta_s - \theta_r)} = \frac{1}{[1 + (\alpha |\psi|)^n]^{1 - 1/n'}}$$

$$\tag{4}$$

where $|\psi|$ is the matric suction, θ_r is residual water content, θ_s is the saturated water content, α is related to the air-entry pressure, and n is related to pore size distribution. Translated to imaging parameters, S_e can be interpreted as the relative pore volume below a threshold pore size. In our study θ_r is below imaging resolution and hence assumed to be 0. θ_s is the total volume of pores and $|\psi|$ is inversely related to pore size through the Young-Laplace equation. Therefore, the inverse of the pore size is used as a proxy for $|\psi|$ and has a unit of $[\frac{1}{L}]$, in which case the resulting α has the unit of L. Alternatively for comparison, the Brooks-Corey model was applied, where water release curve is given by

$$S_e = (\psi/\psi_b)^{-\lambda},\tag{5}$$

where ψ is the matric potential, ψ_b is the air-entry pressure, and λ is the pore size distribution. Experimental data were fitted to the models using a least-square fit in Matlab.

Statistical analysis

Statistical analysis was performed in Matlab 2016a. Data were checked for normality using Shapiro-Wilk test. Statistical differences between group-means were analysed using analysis of variance (ANOVA) with Fisher's Least Significant Differences (LSD) for post-hoc multiple comparisons. For analysis of group-means between two groups, independent two-sample t-test was applied. In all statistical tests, a significance level of P=0.05 was applied.

Data availability

All data supporting this study are available on request from the University of Southampton repository at https://doi.org/xxxx/soton/yyyy.

Results

Plant performance and soil water content measurements

Results of the plant measurements are summarized in Table 1. The NRH genotype had about 40% more shoot fresh mass (F=15.18, P<0.05) and shoot length (F=23.93, P<0.05) than the WT, while the watering treatment had no significant effect on both fresh mass (F=0.08, p=0.77) and shoot length (F=0.39, P<0.39). The average gravimetric water content at the time of the scans was 25.6 \pm 1.4% in the wet treatment, and 24.5 \pm 2.5% in the wet-dry treatment, differences were not statistically significant (paired t-test, p=0.18). Average root hair length of WT plants on micrographs was 521 \pm 230 µm (n=18 root hairs), the maximum recorded length was 991 µm. Root hair density was 50.7 \pm 3.7 hairs mm⁻¹ root length.

Detectable pore volume fraction

Planted treatments (NRH and WT) had a greater mean total pore volume fraction (ϕ) than the unplanted controls (F=8.74, P<0.05), while moisture treatments had no impact (F=1.42, p=0.24) (Figure 3). Multiple comparison of plant treatments showed that the unplanted controls had significantly smaller ϕ (0.39 ± 0.01) than both planted treatments (Fisher's LSD, P<0.05), but there was no significant difference between NRH (0.42 ± 0.01) and WT barley (0.41 ± 0.01).

Within the planted conditions, average ϕ showed variation with distance from the root surface (Figure 4). Despite large variance between individual replicates, Figure 4 indicates a trend showing an initial decrease of average ϕ within 0 to ~0.3 mm from the root surface where a minimum ϕ is reached. Further away from the root (0.3 to 1 mm) the average ϕ seems to increase slightly. Comparison of individual replicates showed that the decrease of ϕ near the root was observed in almost all of the replicates, while the increase of ϕ further away from the root was only seen in some cases (Figure 5, blue circles). Fitting of the ϕ with Dexter's model (Equation 3, Figure 5, green dashed lines, average L2 norm = 0.041) yielded poorer fits than fitting the new model (Equation 1, Figure 4, orange solid lines, average L2 norm = 0.028). The resulting fitting parameters are summarised in Table 2. Individual fitting parameters were uncorrelated and showed no significant differences between treatments.

The fitted curves almost uniformly displayed increased ϕ at the soil-root interface, which was not in all cases supported by the data (see replicate 2 of WT wet-dry in Figure 4). Away from the root a decrease in ϕ was observed with minimum ϕ at a distance of approx. 0.25 mm. At distances further away from the root surface, two distinct patterns were observed. (i) PVF either remained constant at minimum ϕ , which was reflected by corresponding decay constants of k > 1 and ϕ was equal to bulk porosity ϕ_b . (ii) PVF increased away from the root and tended towards ϕ_b , which was reflected by decay constants of k < 1. It is worth noting that the measured ϕ displayed conspicuous oscillations with distance in some of the samples (see e.g. Reps 4 and 5 from *WT wet* in Figure 4).

Pore size distribution

The overall pore size distribution within the imaged region was relatively narrow (Figure 6). On average 38.7 ± 1.6% of the pore volume had a pore diameter between 15-20 µm, followed by the pores between 20-25 µm, which amounted to 28.5 ± 1.1% of the pore volume. Two-way ANOVA with the two fixed effects 'moisture' (2 levels) and 'genotype' (3 levels including the unplanted controls) revealed that the *wet-dry* moisture treatment had a 2% smaller mean fraction of pores between 15-20 µm (F=4.52, P<0.05) and a 1.5% greater mean fraction of pores between 25-30 µm (F=6.78, P<0.05), indicating that the *wet-dry* treatment led to a broader pore size distribution. The 'genotype' had a significant effect on the pores between 5-10 µm (F=17.53, P<0.05), while the unplanted control had a significantly greater fraction (~0.2%) of these pores than both planted conditions (LSD P<0.05). Pores between 20-25 µm were also significantly affected by the 'genotype' (F=7.25, P<0.05), while the controls had a 2% smaller fraction of these pores than the planted conditions (LSD P<0.05). The controls had as a 1.6% greater fraction of pores between 25-30 µm (F=4.06, P<0.05; LSD P<0.05) and a 1.6% greater fraction of pores between 30-35 μ m (F=672, P<0.05; LSD P<0.05). There were no significant differences between the two genotypes NRH and WT. Overall, these results indicate increases in larger pores in the controls relative to the planted treatments, while also the smallest pore size class was significantly increased.

Fitting of the pore size distribution was better with the van Genuchten equation (average L2 norm = 0.1) compared to the Brooks-Corey formulation (L2 norm = 0.36). Therefore, the van Genuchten approach was used to analyse the pore size distributions. Resulting fitting parameters for the entire scanned regions are summarised in Table 3. The van Genuchten parameter α was significantly decreased by the moisture treatment (F=4.39, P<0.05), indicating a relatively smaller pore size in the wet treatment, but was unaffected by the plant treatment including unplanted controls (F=1.55, p=0.23). Plant treatment had a significant effect on van Genuchten n (F=5.33, P<0.05). Fisher's LSD indicated that the control treatment had a significantly smaller n (P<0.05) than the planted treatments, with no difference between the contrasting genotypes. Moisture treatment had no significant effect on van Genuchten n (F=2.7, p=0.11). Within the planted treatments, the pore size distribution shifted to relatively larger pores (mean pore size at the soil-root interface surface 16.74 \pm 0.60 μ m and 18.02 \pm 0.85 μ m at 1 mm distance) and a wider pore size distribution with distance from the roots (Figure 7). Van Genuchten α increased linearly between 0 mm and 1 mm distance from the root (Figure 8a), indicating relatively smaller pores near the root, while van Genuchten ndecreased exponentially between 0 and 1 mm distance (Figure 8b), indicating a narrower pore size distribution near the root.

Discussion

This study has contrasting findings to our previous work where root hairs were observed to increase detectable porosity (Koebernick et al., 2017) and many studies that observed significant increases to macroporosity due to the presence of roots (Feeney et al., 2006; Whalley et al., 2005). However, the current study used soil sieved to < 250 μ m, whereas previous research used soil sieved to < 2 mm (e.g. Feeney et al., 2006; Helliwell et al., 2017; Koebernick et al., 2017). Our smaller particle size and the resulting packing condition produced a soil environment more typical of intraggregate structure. At 2 mm size, aggregated structures are more apparent and roots were observed to preferentially grow in between these aggregates (Koebernick et al. 2017). Soil in the syringe barrels was at 1.3 Mg m⁻³, but other research used a looser 1.2 Mg m⁻³.

Despite the presence of root hairs having no observable impact on porosity formation, the presence of roots had a major impact. Presence of roots significantly increased the total detectable pore volume fraction and narrowed the pore size distribution. Whereas the narrowed pore size distribution likely resulted from compression by the root decreasing larger pores (Kutilek et al., 2006), the increased detectable porosity probably resulted from the combined activity of roots and soil microbiota, as reported in earlier studies (Feeney et al. 2006; Hallett et al. 2009). In the work by Hallett et al. (2009) the macropore size increased in the rhizosphere, similar to the findings of Whalley et al. (2005) on rhizosheath soil aggregates.

Plants were also significantly older in previous studies (Feeney et al. 2006; Hallett et al. 2009; Whalley et al. 2005), hence the differences may reflect temporal dynamics in the rhizosphere rather than contradictory evidence. It may also be that root hair extension was restricted by the lack of macropores in the rhizosphere in our study: Bengough et al. (2016) found that root hairs did not increase maize root anchorage (as compared with hairless mutants) when soil density increased to 1.3 Mg m⁻³ or greater using soil (though sieved to <2mm) from the same field as our study. Although this suggests restricted root hair growth, we found an average root hair density of 50.7 mm⁻¹ taken from micrographs.

The present study confirms previous observations of increased pore volume fraction at the soil-root interface (Helliwell et al. 2017; Koebernick et al. 2017). The radial porosity distribution about the root surface showed very different patterns for individual replicates suggesting that even in a relatively homogeneous soil there can be very different porosity distributions for individual roots. This was especially true for the degree of soil compaction. Compelling evidence for significant increases in soil density (corresponding to a decay constant of k < 1) was only observed in roughly half of the replicates. In contrast, an increased pore volume at the soil-root interface was observed almost universally. The proposed formulation of porosity variation (Eq. 1), which accounts for the surface/wall effect at the root soil interface, fitted the experimental data well in the majority of cases (average L2 norm = 0.028), despite the oversimplification of using a mono-sized sphere packing. This oversimplification is however reflected in somewhat empirical fitting parameters – namely the particle radius r_p , which was about 4-fold greater than the aperture of the sieve (r=125 μ m). We note that, for the sake of simplicity, the model used a Cartesian coordinate system, i.e. the root surface was represented by a plane surface. Therefore, the area over which porosity is increased, as well as the amplitude, should only depend on r_p . The assumption is that r_0 is much larger than r_p . It may be argued that this is not true in the present case, but it was decided to keep the model as simple as possible. The overestimation of r_p compared to the sieve aperture may

indicate the formation of aggregates near the root surface. Undoubtedly, the soil particles in the experiment, which are non-spherical, polydispersed, and randomly packed, deviate significantly from the modelled spheres, therefore r_p is only to some extent a physical parameter. Theoretically, mono-sized spheres are the worst-packing objects among all convex shapes in 3D (Baule and Makse 2014), although the model used packing on a regular lattice and porosities would be greater for random packings, which would be expected to occur in soil. The occurrence of oscillations of pore volume with distance from the root found in some of the data sets, indicates that the assumption of the spherical nature of the particles was a fair assumption. Such oscillations are observed when packing spheres or regularly shaped particles (Mueller 2010), but are not observed for highly irregular shapes (Roblee et al. 1958). The large values of r_p are partially a result of the combined packing and compaction effect in Eq. 1. When compaction is minimal (e.g. replicate 1 of WT wet-dry in Fig. 5 and Table 2), the minimum porosity is reached closer to the computed r_p value than in cases with appreciable compaction (e.g. replicate 4 of WT wet-dry in Fig. 5 and Table 2). In our model, the surface packing term assumes rigid particles, while the Dexter type compaction decreases the porosity due to the assumption of continuum deformation. This leads to the discrepancy between r_p and the radial distance of minimum porosity. Figure 5 shows that minimum porosity was reached at 2 250 μ m in most cases, which is about twice as large as the sieve aperture radius. This may be an indication of aggregation of individual particles at the root plane. Root and microbial derived mucilage are thought to play an important role in aggregate formation in the rhizosphere (Caravaca et al. 2005; Moreno-Espíndola et al. 2007; Vidal et al. 2018). Barley exudates initially disperse and then gel soil (Naveed et al. 2017a; Naveed et al. 2017b), so the observed extension of the packing effect beyond the initial sieved soil size was likely due to aggregation. The mixed phase was assumed unaffected by the roots in the present model because of the limiting imaging resolution. It has to be noted that clay particle organisation can be affected by roots (Dorioz et al. 1993; Vidal et al. 2018) which might produce variations in pore volume that cannot be captured by the present model.

Further away from the root, beyond r_p , porosity increased in some of the replicates, indicating some degree of soil compaction closer to the root, while in other replicates the porosity remained constant – at least within the analysed 1-mm distance from the root. One possible explanation is that compression in these samples may have extended further away from the roots. This could not be analysed because this region extended into the zone that was affected by imaging artefacts. We note that the age of the imaged roots was not controlled (beyond scanning at the same depth of the syringe barrels to minimise the variation of root age). Some of the observed differences may therefore be a result of a temporal change in rhizosphere structure along the roots. Temporally resolved imaging, such as in Helliwell et al. (2017), showed that porosity at the soil-root interface

changed significantly with age. Such an age related effect is also conceivable further away from the roots, for example through microbial degradation of root exudates, which may change soil physical properties (Naveed et al. 2017a). The variation of pore volume with distance from the root in this study was quite different to the observations in a similar previous study, which used the same genotypes, but a more heterogeneous soil structure (Koebernick et al. 2017). The previous study showed increased fraction of air-filled pores at the root surface for the WT genotype, while for the NRH mutant, air-filled porosity decreased near the root. The differences are partially explained by the different segmentation approaches in the two studies. While Koebernick et al. (2017) segmented the soil into three phases – solid mineral particles, air-filled pores, and a mixed phase comprising water filled pores and sub-resolution soil particles, the present study only distinguishes two (i.e. solid and pore) phases. A proportion of the voxels that were classified as pore in the present study, particularly the smaller pores, were part of the mixed phase in Koebernick et al. (2017), which indeed showed an increased volume fraction near the root surface of both genotypes. The main difference is therefore the lack of a genotype effect on pore structure in the present study. For the finer textured soil used here, root hairs seemed to have no significant effect on pore structure. These differences show that putative hair-induced changes to soil structure as observed in Koebernick et al. (2017) are influenced by the soil characteristics. Barley roots have been shown to produce longer root hairs in coarser soils (Haling et al. 2014), which may also go some way to explaining the lack of a genotype effect in the present study where the root hair length is substantially shorter than seen in the more coarsely sieved soil (Brown et al. 2012) and in model soils of a range of textural sizes (Haling et al. 2014).

In contrast, the previous study by Koebernick et al. (2017) did not show a significant change of pore size distribution, which was only analysed for the air-filled pores, with distance from the root. Here, the pore size distribution clearly showed an increased frequency of smaller pores at the expense of larger pores at the root surface. An increased frequency of smaller pores indicates soil compression (Kutílek et al. 2006; Leij et al. 2002). Shifts in pore size distribution as affected by root growth in the field can show substantial variability with different root morphologies. While coarse root systems have been shown to increase macroporosity (Bodner et al. 2014; Holtham et al. 2007), fine root systems increased the frequency of the smaller pore fractions (Bodner et al. 2014). It was suggested that a finer root systems can use the available pore space more effectively as preferential growth paths and shifting the pore-size distribution towards smaller pores via in-growth into the larger pores (Bodner et al. 2014). Here, we show that in a much finer textured growth medium, which provides no large macropores as preferential growth paths, a shift towards smaller pore sizes can be observed within the rhizosphere, most likely due to aggregate coalescence and compression.

Despite this, pore volume fraction is larger near the root surface, which is explained by a wall effect that causes incomplete packing of the larger, incompressible mineral particles which are displaced by the growing root.

Our results provide evidence that soil structural parameters are significantly altered by root activity. In contrast to previous work (Koebernick et al. 2017) that used a more heterogeneous soil, different genotypes with contrasting root hair morphology did not affect the pore structure in the rhizosphere. In line with our earlier argument that the structure in the present study resembled intragreggate pore structure we conclude that presence of hairs on barley roots is more likely to affect inter-aggregate pore structure. Roots increased the frequency of smaller pores close to the root surface accompanied by an increase in total pore volume fraction. These changes could have important implications on water and solute uptake by roots, as the enhanced total volume of pores and the shift towards smaller pores might increase the unsaturated hydraulic conductivity in the rhizosphere, particularly at drier water potentials when the soil is most limiting.

Acknowledgments

NK, LJC, TR and IS are funded by BBSRC SARISA BB/L025620/1. KRD is funded by ERC 646809DIMR. LKB, PDH, TSG, MN and AR are funded by BBSRC BB/J00868/1 and AGB is funded by BB/L025825/1. The James Hutton Institute receives financial support from the Rural & Environment Science & Analytical Services Division of the Scottish Government. IS and TR are also funded by EPSRC EP/M020355/1. TR is also funded by ERC 646809DIMR, BBSRC SARIC BB/P004180/1 and NERC NE/L00237/1. The authors acknowledge the use of the I13 beamline at Diamond Light Source, Oxfordshire, UK (Experiment MT12525). We would like to thank Dr. Shashidara Marathe and Dr. Silvia Cipiccia, who provided considerable help during our beamtime. We would also like to thank Ian Sinclair for advice in preparation of the beamtime and Mike Ogden for help at the beamline.

Tables

Table 1 Plant (Hordeum vulgare cv. Optic) performance measurements at the time of scanning.

Treatment	Shoot mass	Shoot
	(fresh)	length
	(g)	(mm)
WT wet	0.127±0.04	104.0±34.9
NRH wet	0.194±0.03	165.9±12.1
WT wet-dry	0.129±0.02	118.2± 7.0
NRH wet-dry	0.181±0.04	161.7±29.3

Data are mean ± SD. WT, wild-type plant; NRH, hairless plant.

Table 2 Fitted parameters of the modified model (Eqn 2).

	Condition	Replicate	ϕ_b	k	r_0	r_p	ϕ_m
	NRH wet	1	0.399	0.29	306.4	535.4	0.413
		2	0.373	1.06	306.7	523.0	0.427
		3	0.388	1.85	371.0	430.1	0.061
		4	0.386	1.95	342.3	435.4	0.221
		5	0.402	1.26	306.5	1120.9	0.214
		Mean	0.390	1.28	326.6	609.0	0.267
		SD	0.010	0.60	26.2	259.6	0.137
	WT wet	1	0.389	1.88	341.4	381.9	0.052
		2	0.392	0.29	306.4	546.2	0.214
		3	0.408	0.31	306.4	439.6	0.373
		4	0.381	0.35	306.4	579.6	0.373
		5	0.373	0.79	306.4	758.4	0.352
		Mean	0.389	0.73	313.4	541.1	0.273
		SD	0.012	0.60	14.0	129.9	0.125
	NRH wet-dry	1	0.407	0.81	352.2	417.8	0.151
Y		2	0.402	0.51	341.2	547.2	0.363
		3	0.429	2.87	340.5	260.7	0.414
		4	0.395	0.22	306.4	618.3	0.129
		5	0.398	1.63	306.6	2521.9	0.396
		Mean	0.406	1.21	329.4	873.2	0.291
		SD	0.012	0.96	19.2	833.3	0.124

WT wet-dry	1	0.347	1.40	334.9	565.8	0.031
	2	0.400	1.79	345.0	346.8	0.188
	3	0.412	2.86	308.7	485.0	0.267
	4	0.418	0.21	306.4	604.8	0.066
	Mean	0.394	1.57	323.8	500.6	0.138
	SD	0.028	0.95	16.6	98.8	0.095

 ϕ_b is the bulk porosity, k is the Dexter decay constant, r_0 is the root radius, r_p is the particle radius, and ϕ_m is the mixed phase porosity. Plant (*Hordeum vulgare* cv Optic). WT, wild-type plant; NRH, hairless plant.

Table 3 Average (± SD) modified van Genuchten parameters fitted to the pore size distributions of the CT scanned regions of interest for the different conditions.

Condition	α	n
NRH wet	18.04 ± 0.4	6.83 ± 0.2
WT wet	17.87 ± 0.32	7.08 ± 0.16
Control wet	18.05 ± 0.43	6.72 ± 0.46
NRH wet-dry	18.27 ± 0.43	6.9 ± 0.32
WT wet-dry	18.08 ± 0.37	6.85 ± 0.17
Control wet-dry	18.64 ± 0.46	6.24 ± 0.34

Plant (Hordeum vulgare cv Optic). WT, wild-type plant; NRH, hairless plant.

Figure captions

Figure 1: Schematic drawing of the variation in soil porosity adjacent to the root surface. At a distance r between the root radius r_0 and the particle radius r_p , porosity $\phi(r)$ is affected by the packing geometry of the spherical particles at the root surface. Immediately adjacent to the root, the porosity equals the mixed phase porosity ϕ_m . If there is no Dexter compression the porosity approaches the bulk porosity ϕ_b at r_p . Further oscillation of porosity at $r > r_p$ is not considered in the model. Note that the schematic drawing is 2D, while the model and the graph shown on the right consider 3D sphere packing.

Figure 2: Horizontal slice of a CT scanned barley root growing in a soil-filled syringe barrel showing the main image processing steps. (a) 8-bit grey-scale image after histogram equalization; (b) segmented root, white is the detected root structure, black is background; (c) Otsu segmentation, solid soil particles are shown in white, pore space is shown in black; (d) local thickness of the pore space. Colours indicate local pore diameter in μ m. Solid particles and the masked out root structure is shown in black. Bars, 1 mm.

Figure 3: Total pore volume fraction (PVF) in the CT scanned region of interest in the barley rhizosphere. Control treatment had significantly smaller PVF than wild-type (WT) and no root hair (NRH) treatments (2-way ANOVA *P*<0.05, Fisher's LSD *P*<0.05). Moisture treatment (wet vs wet-dry) had no significant effect on PVF. Error bars show + SD: significant difference: *, *P*<0.05.

Figure 4: Mean pore volume fraction (PVF) \pm SD with distance from the barley root surface for the different conditions including no root hair (NRH) and wild-type (WT) genotypes with both wet and wet-dry watering treatments. Each data point is the mean PVF within an annulus of 32 μ m thickness for each condition.

Figure 5: Comparison of pore volume fraction ϕ with distance from the barley root fitted using Dexter's model (green dashed lines) and the new model (Eqn 1, orange lines). Replicates 1–5 of each condition are plotted on the same line from left to right. Treatments include no root hair (NRH) and wild-type (WT) genotypes with both wet and wet-dry watering treatments Figure 6: Pore size distribution of the barley rhizosphere in the CT scanned region of interest binned into 5- μ m wide classes. Each bar represents the relative fraction of the total pore volume by each pore size class within the different conditions ± SD. Pore size classes are indicated by the black and white bars at the bottom. Treatments include unplanted control, no root hair (NRH) and wild-type (WT) genotypes with both wet and wet-dry watering treatments.

Figure 7: Cumulative pore size distribution in the barley rhizosphere fitted with the van Genuchten equation. Different colours indicate different distances (<1 mm) from the root surface. Data in this plot are obtained from the wild-type (WT) wet-dry treatment, replicate 3.

Figure 8: Modified van Genuchten parameters of the pore size distribution over distance from the barley root surface. Average van Genuchten parameters (α on the left panel and n on the right panel) over the entire imaged region are shown in Table 3. Data points represent the fitted van Genuchten parameters for each replicate within 32-µm wide annuli with increasing distance from the root surface while the model curve is represented by the red dashed line.

Author contributions

NK, SDK, PDH, TSG, AGB, and TR designed the study. NK, SDK, AR, PDH, AGB, TSG, LKB, MN, LJC collected the data. NK analysed the data and drafted the manuscript. KRD and NK developed the model. NK wrote the manuscript and all other authors provided critical revision and approval before submission and publication. PDH was PI on funding from the BBSRC and the Diamond Light Source Experiment MT12525.

References

- Albalasmeh AA, Ghezzehei TA (2014) Interplay between soil drying and root exudation in rhizosheath development. Plant and Soil 374: 739-751. doi: 10.1007/s11104-013-1910-y.
- Aravena JE, Berli M, Ghezzehei TA, Tyler SW (2011) Effects of root-induced compaction on rhizosphere hydraulic properties--X-ray microtomography imaging and numerical simulations. Environ Sci Technol 45: 425-431. doi: 10.1021/es102566j.
- Aravena JE, Berli M, Ruiz S, Suárez F, Ghezzehei TA, Tyler SW (2014) Quantifying coupled deformation and water flow in the rhizosphere using X-ray microtomography and numerical simulations. Plant and Soil 376: 95-110. doi: 10.1007/s11104-013-1946-z.
- Baule A, Makse HA (2014) Fundamental challenges in packing problems: from spherical to nonspherical particles. Soft Matter 10: 4423-4429.
- Bengough AG, Loades K, McKenzie BM (2016) Root hairs aid soil penetration by anchoring the root surface to pore walls. Journal of Experimental Botany 67: 1071-1078. doi: 10.1093/jxb/erv560.
- Bengough AG, McKenzie BM, Hallett PD, Valentine TA (2011) Root elongation, water stress, and mechanical impedance: a review of limiting stresses and beneficial root tip traits. Journal of Experimental Botany 62: 59-68. doi: 10.1093/jxb/erq350.
- Bingham IJ, Bengough AG (2003) Morphological plasticity of wheat and barley roots in response to spatial variation in soil strength. Plant and Soil 250: 273-282. doi: 10.1023/A:1022891519039.
- Bodner G, Leitner D, Kaul H-P (2014) Coarse and fine root plants affect pore size distributions differently. Plant and Soil 380: 133-151. doi: 10.1007/s11104-014-2079-8.
- Brown LK, George TS, Thompson JA, Wright G, Lyon J, Dupuy L, Hubbard SF, White PJ (2012) What are the implications of variation in root hair length on tolerance to phosphorus deficiency in combination with water stress in barley (*Hordeum vulgare*)? Annals of Botany 110: 319-328. doi: 10.1093/aob/mcs085.
- Bruand A, Cousin I, Nicoullaud B, Duval O, Bégon JC (1996) Backscattered electron scanning images of soil porosity for analyzing soil compaction around roots. Soil Science Society of America Journal 60: 895-901. doi: 10.2136/sssaj1996.03615995006000030031x.
- Caldwell DG, McCallum N, Shaw P, Muehlbauer GJ, Marshall DF, Waugh R (2004) A structured mutant population for forward and reverse genetics in Barley (*Hordeum vulgare* L.). The Plant Journal 40: 143-150. doi: 10.1111/j.1365-313X.2004.02190.x.
- Caravaca F, Alguacil MM, Torres P, Roldán A (2005) Plant type mediates rhizospheric microbial activities and soil aggregation in a semiarid Mediterranean salt marsh. Geoderma 124: 375-382. doi: http://dx.doi.org/10.1016/j.geoderma.2004.05.010.
- Carminati A, Vetterlein D, Koebernick N, Blaser S, Weller U, Vogel H-J (2013) Do roots mind the gap? Plant and Soil 367: 651-661. doi: 10.1007/s11104-012-1496-9.
- Chimungu JG, Loades KW, Lynch JP (2015) Root anatomical phenes predict root penetration ability and biomechanical properties in maize (*Zea mays*). Journal of Experimental Botany 66: 3151-3162. doi: 10.1093/jxb/erv121.

- Colombi T, Braun S, Keller T, Walter A (2017) Artificial macropores attract crop roots and enhance plant productivity on compacted soils. Science of The Total Environment 574: 1283-1293. doi: https://doi.org/10.1016/j.scitotenv.2016.07.194.
- Czarnes S, Hallett PD, Bengough AG, Young IM (2000) Root- and microbial-derived mucilages affect soil structure and water transport. European Journal of Soil Science 51: 435-443. doi: 10.1046/j.1365-2389.2000.00327.x.
- Dexter AR (1987) Compression of soil around roots. Plant and Soil 97: 401-406. doi: 10.1007/BF02383230.
- Dorioz JM, Robert M, Chenu C (1993) The role of roots, fungi and bacteria on clay particle organization. An experimental approach. *Geoderma* **56**: 179–194.
- Feeney DS, Crawford JW, Daniell T, Hallett PD, Nunan N, Ritz K, Rivers M, Young IM (2006) Three-dimensional microorganization of the soil–root–microbe system. Microbial Ecology 52: 151-158. doi: 10.1007/s00248-006-9062-8.
- Haling RE, Brown LK, Bengough AG, Valentine TA, White PJ, Young IM, George TS (2014) Root hair length and rhizosheath mass depend on soil porosity, strength and water content in barley genotypes. Planta 239: 643-651. doi: 10.1007/s00425-013-2002-1.
- Hallett PD, Feeney DS, Bengough AG, Rillig MC, Scrimgeour CM, Young IM (2009) Disentangling the impact of AM fungi versus roots on soil structure and water transport. Plant and Soil 314: 183-196. doi: 10.1007/s11104-008-9717-y.
- Helliwell JR, Sturrock CJ, Mairhofer S, Craigon J, Ashton RW, Miller AJ, Whalley WR, Mooney SJ (2017) The emergent rhizosphere: imaging the development of the porous architecture at the root-soil interface. Scientific Reports 7: 14875. doi: 10.1038/s41598-017-14904-w.
- Hettiaratchi DRP (1990) Soil compaction and plant root growth. Philosophical Transactions of the Royal Society of London Series B: Biological Sciences 329: 343-355. doi: 10.1098/rstb.1990.0175.
- Holtham DAL, Matthews GP, Scholefield DS (2007) Measurement and simulation of void structure and hydraulic changes caused by root-induced soil structuring under white clover compared to ryegrass. Geoderma 142: 142-151. doi: https://doi.org/10.1016/j.geoderma.2007.08.018.
- Iijima M, Higuchi T, Barlow PW, Bengough AG (2003) Root cap removal increases root penetration resistance in maize (*Zea mays* L.). Journal of Experimental Botany 54: 2105-2109. doi: 10.1093/jxb/erg226.
- Jin K, Shen J, Ashton RW, Dodd IC, Parry MAJ, Whalley WR (2013) How do roots elongate in a structured soil? Journal of Experimental Botany 64: 4761-4777. doi: 10.1093/jxb/ert286.
- Keyes S, Cooper L, Koebernick N, Duncan Simon J, McKay Fletcher Daniel M, Scotson C, van Veelen A, Sinclair I, Roose T (2017) Measurement of micro-scale soil deformation around roots using 4D synchrotron tomography and image correlation. RS Interface 14: 20170560.
 DOI: 10.1098/rsif.2017.0560
- Keyes SD, Daly KR, Gostling NJ, Jones DL, Talboys P, Pinzer BR, Boardman R, Sinclair I, Marchant A, Roose T (2013) High resolution synchrotron imaging of wheat root hairs growing in soil and image based modelling of phosphate uptake. New Phytol 198: 1023-1029. doi: 10.1111/nph.12294.
- Koebernick N, Daly KR, Keyes SD, George TS, Brown LK, Raffan A, Cooper LJ, Naveed M, Bengough AG, Sinclair I, Hallett PD, Roose T (2017) High-resolution synchrotron imaging shows that root hairs influence rhizosphere soil structure formation. New Phytol 216: 124-135. doi: 10.1111/nph.14705.
- Kooistra MJ, Schoonderbeek D, Boone FR, Veen BW, Van Noordwijk M (1992) Root-soil contact of maize, as measured by a thin-section technique. Plant and Soil 139: 119-129. doi: 10.1007/bf00012849.
- Kutílek M, Jendele L, Panayiotopoulos KP (2006) The influence of uniaxial compression upon pore size distribution in bi-modal soils. Soil and Tillage Research 86: 27-37. doi: http://dx.doi.org/10.1016/j.still.2005.02.001.
- Leij FJ, Ghezzehei TA, Or D (2002) Modeling the dynamics of the soil pore-size distribution. Soil and Tillage Research 64: 61-78. doi: http://dx.doi.org/10.1016/S0167-1987(01)00257-4.

Moreno-Espíndola IP, Rivera-Becerril F, de Jesús Ferrara-Guerrero M, De León-González F (2007) Role of root-hairs and hyphae in adhesion of sand particles. Soil Biology and Biochemistry 39: 2520-2526. doi: http://dx.doi.org/10.1016/j.soilbio.2007.04.021.

Mueller GE (2010) Radial porosity in packed beds of spheres. Powder Technology 203: 626-633.

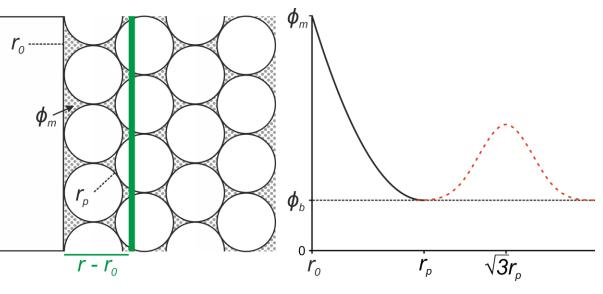
- Mwafulirwa L, Baggs EM, Russell J, George T, Morley N, Sim A, de la Fuente Cantó C, Paterson E (2016) Barley genotype influences stabilization of rhizodeposition-derived C and soil organic matter mineralization. Soil Biology and Biochemistry 95: 60-69. doi: https://doi.org/10.1016/j.soilbio.2015.12.011.
- Naveed M, Brown L, Raffan A, George T, Bengough A, Roose T, Sinclair I, Koebernick N, Cooper L, Hallett P (2017a) Plant exudates can either stabilise or weaken soils depending on species, origin and time. European Journal of Soil Science 68, 806–816, doi: 10.1111/ejss.12487
- Naveed M, Brown L, Raffan A, George T, Bengough A, Roose T, Sinclair I, Koebernick N, Cooper L, Hallett P (2017b) Rhizosphere-scale quantification of hydraulic and mechanical properties of soil impacted by root and seed exudates. Vadose Zone Journal. 17: doi:10.2136/vzj2017.04.0083
- Otsu N (1979) A threshold selection method from gray-level histograms. IEEE transactions on systems, man, and cybernetics 9: 62-66.
- Richards L, Wadleigh C (1952) Soil water and plant growth. In 'Soil physical conditions and plant growth'.(Ed. BT Shaw) pp. 74–251. American Society of Agronomy Series Monographs, Volume II. Academic Press: New York, NY.
- Roblee L, Baird R, Tierney J (1958) Radial porosity variations in packed beds. AIChE Journal 4: 460-464.
- Ruiz S, Or D, Schymanski SJ (2015) Soil penetration by earthworms and plant roots—mechanical energetics of bioturbation of compacted soils. PLOS ONE 10: e0128914. doi: 10.1371/journal.pone.0128914.
- Schindelin J, Arganda-Carreras I, Frise E, Kaynig V, Longair M, Pietzsch T, Preibisch S, Rueden C, Saalfeld S, Schmid B (2012) Fiji: an open-source platform for biological-image analysis. Nature methods 9: 676-682.
- Schmidt S, Bengough AG, Gregory PJ, Grinev DV, Otten W (2012) Estimating root–soil contact from 3D X-ray microtomographs. European Journal of Soil Science 63: 776-786. doi: 10.1111/j.1365-2389.2012.01487.x.
- Suzuki M, Shinmura T, Iimura K, Hirota M (2008) Study of the wall effect on particle packing structure using X-ray micro computed tomography. Advanced Powder Technology 19: 183-195. doi: https://doi.org/10.1163/156855208X293817.
- Valentine TA, Hallett PD, Binnie K, Young MW, Squire GR, Hawes C, Bengough AG (2012) Soil strength and macropore volume limit root elongation rates in many UK agricultural soils. Annals of Botany 110: 259-270. doi: 10.1093/aob/mcs118.
- Vidal A, Hirte J, Bender SF, Mayer J, Gattinger A, Höschen C, Schädler S, Iqbal TM, Mueller CW (2018) Linking 3D soil structure and plant-microbe-soil carbon transfer in the rhizosphere. Frontiers in Environmental Science 6. doi: 10.3389/fenvs.2018.00009.
- Vollsnes AV, Futsaether CM, Bengough AG (2010) Quantifying rhizosphere particle movement around mutant maize roots using time-lapse imaging and particle image velocimetry. European Journal of Soil Science 61: 926-939. doi: 10.1111/j.1365-2389.2010.01297.x.
- Watt M, McCully ME, Canny MJ (1994) Formation and stabilization of rhizosheaths of *Zea mays* L. (effect of soil water content). Plant Physiology 106: 179-186. doi: 10.1104/pp.106.1.179.
- Whalley WR, Riseley B, Leeds-Harrison PB, Bird NRA, Leech PK, Adderley WP (2005) Structural differences between bulk and rhizosphere soil. European Journal of Soil Science 56: 353-360. doi: 10.1111/j.1365-2389.2004.00670.x.
- Yoshida S, Hallett PD (2008) Impact of hydraulic suction history on crack growth mechanics in soil. Water Resources Research 44, W00C01, doi: 10.1029/2007WR006055.
- Young IM (1998) Biophysical interactions at the root-soil interface: a review. The Journal of Agricultural Science 130: 1-7.

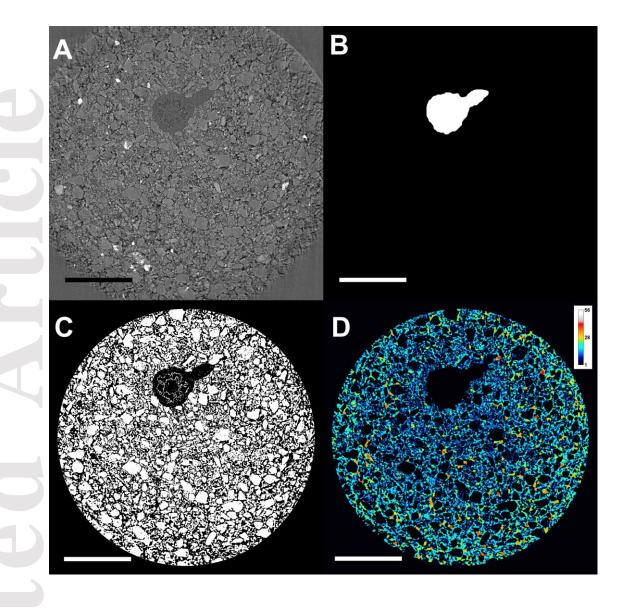
Supplementary Figure Legends

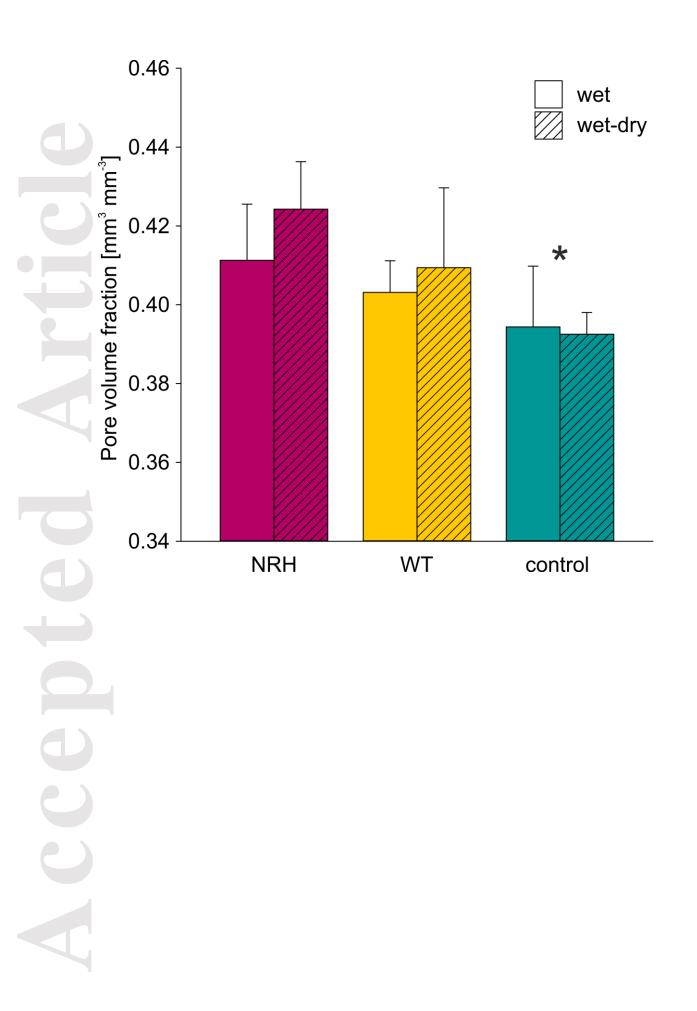
Fig. S1 Plant growth setup showing the experimental design.

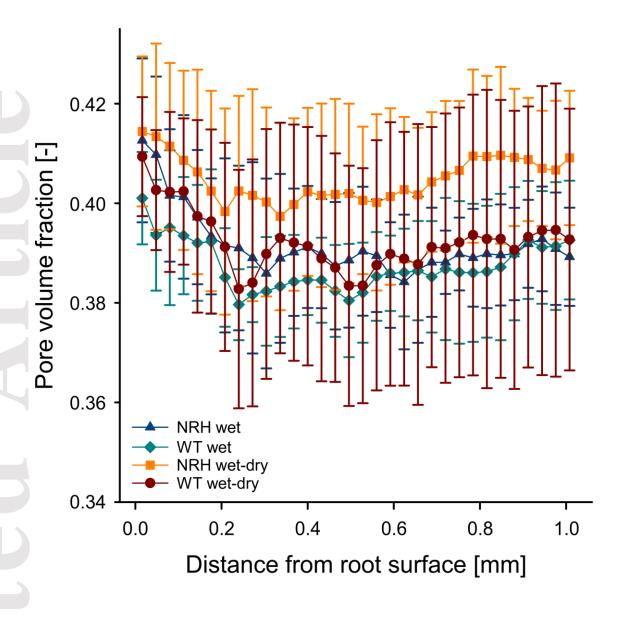
Fig. S2 Projection of the average grey values in the CT scanned barley rhizosphere along the Z-axis.

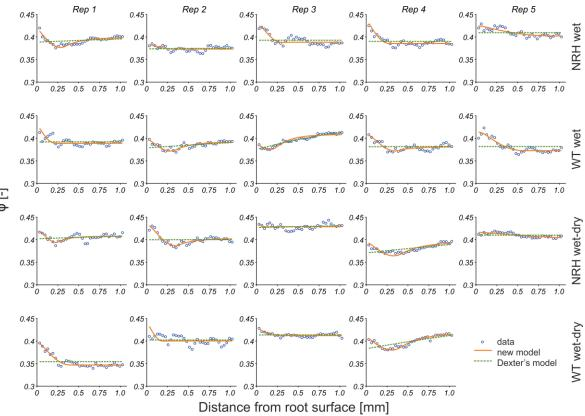
Fig. S3 Cumulative pore size distribution fitted with the Brooks-Corey and van Genuchten equations.











ф [-]

